RhoA downregulation in the murine intestinal epithelium results in chronic Wnt activation and increased tumorigenesis

Dopeso, Higinio; Rodrigues, Paulo; Cartón-García, Fernando; Macaya, Irati; Bilic, Josipa; Anguita, Estefanía; Jing, Li; Brotons, Bruno; Vivancos, Núria; Beà, Laia

Published in:
Iscience

DOI:
10.1016/j.isci.2024.109400

Publication date:
2024

iScience

CellPress
OPEN ACCESS

Article

RhoA downregulation in the murine intestinal epithelium results in chronic Wnt activation and increased tumorigenesis

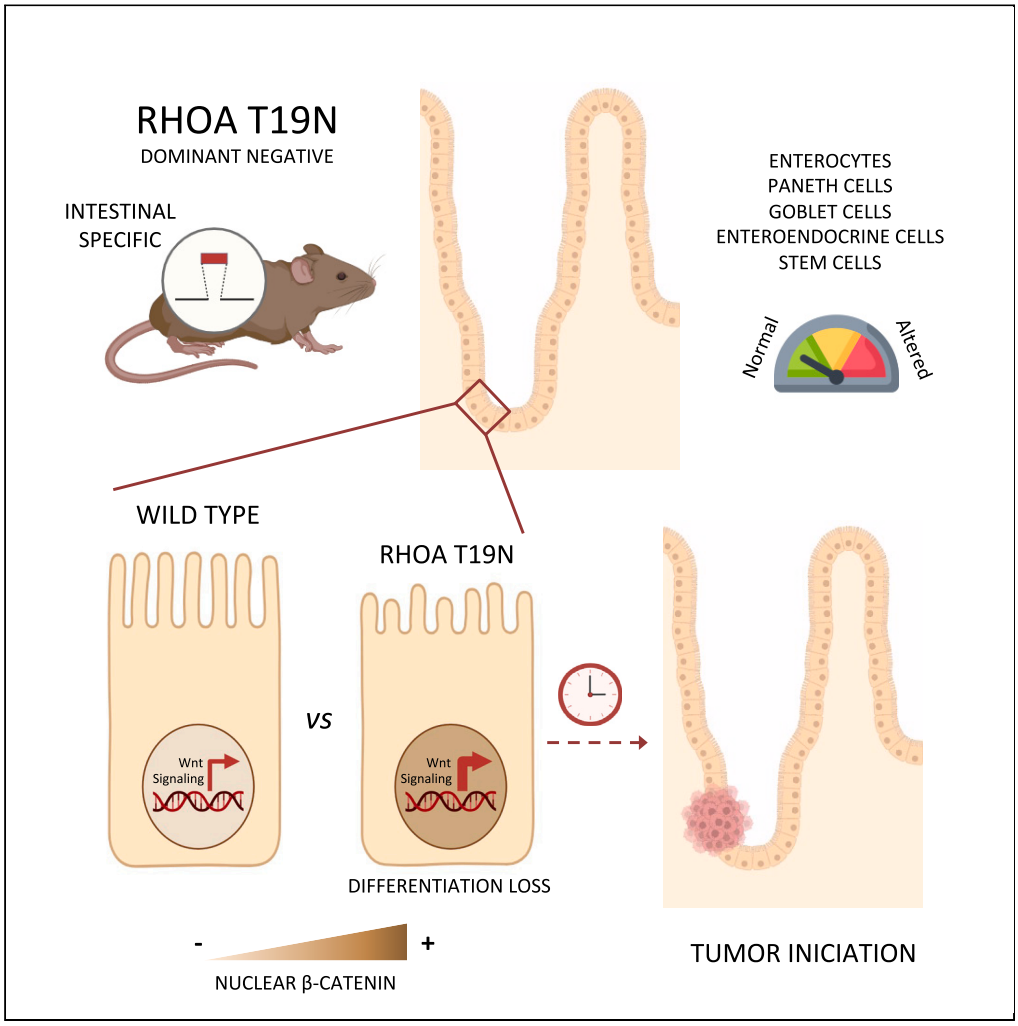

Higinio Dopeso, Paulo Rodrigues, Fernando Cartón-García, ..., Kazuto Kobayashi, Águeda Martinez-Barriocanal, Diego Arango

amartinez@irblleida.cat (Á.M.-B.)
darango@irblleida.cat (D.A.)

Highlights

RhoA downregulation elevates nuclear β-catenin in the intestinal epithelium

RhoA regulates intestinal cell differentiation in mice via Wnt signaling

RhoA inhibition results in increased intestinal tumorigenesis

Dopeso et al., iScience 27, 109400
April 19, 2024
https://doi.org/10.1016/j.isci.2024.109400

iScience

CellPress
OPEN ACCESS

Article

RhoA downregulation in the murine intestinal epithelium results in chronic Wnt activation and increased tumorigenesis

Higinio Dopeso,[1,14] Paulo Rodrigues,[1,14] Fernando Cartón-García,[1] Irati Macaya,[1] Josipa Bilic,[1] Estefanía Anguita,[1,2] Li Jing,[1,2] Bruno Brotons,[2] Núria Vivancos,[2] Laia Beà,[2] Manuel Sánchez-Martín,[3,4,5] Stefania Landolfi,[6,7] Javier Hernandez-Losa,[6,7] Santiago Ramon y Cajal,[6,7] Rocío Nieto,[1] María Vicario,[8] Ricard Farre,[9] Simo Schwartz, Jr.,[10,11] Sven C.D. van Ijzendoorn,[12] Kazuto Kobayashi,[13] Águeda Martinez-Barriocanal,[1,2,*] and Diego Arango[1,2,15,*]

SUMMARY

Rho GTPases are molecular switches regulating multiple cellular processes. To investigate the role of RhoA in normal intestinal physiology, we used a conditional mouse model overexpressing a dominant negative RhoA mutant (RhoA^{T19N}) in the intestinal epithelium. Although RhoA inhibition did not cause an overt phenotype, increased levels of nuclear β-catenin were observed in the small intestinal epithelium of *RhoA^{T19N}* mice, and the overexpression of multiple Wnt target genes revealed a chronic activation of Wnt signaling. Elevated Wnt signaling in *RhoA^{T19N}* mice and intestinal organoids did not affect the proliferation of intestinal epithelial cells but significantly interfered with their differentiation. Importantly, 17-month-old *RhoA^{T19N}* mice showed a significant increase in the number of spontaneous intestinal tumors. Altogether, our results indicate that RhoA regulates the differentiation of intestinal epithelial cells and inhibits tumor initiation, likely through the control of Wnt signaling, a key regulator of proliferation and differentiation in the intestine.

INTRODUCTION

The epithelium lining the lumen of the intestine plays a key role in the digestion and absorption of nutrients and maintains a barrier against potentially harmful substances and pathogens. This simple columnar epithelium is a rapidly proliferating system that undergoes constant renewal.[1,2] All the cells in the intestinal epithelium are derived from slowly proliferating stem cells located at or near the bottom of test tube-shaped invaginations of the epithelial layer known as crypts of Lieberkühn.[1,2] These stem cells divide asymmetrically and give rise to transit-amplifying cells that undergo several rounds of replication before differentiating into one of the four main functional cell types in the intestinal epithelium, namely, absorptive, goblet, enteroendocrine, and Paneth cells.[3–6] With the exception of Paneth cells that reside in the bottom of the small intestinal crypts, differentiated epithelial cells move toward the tip of the small intestinal villi or the flat colonic mucosa where they undergo apoptosis and are eventually shed into the intestinal lumen.[1]

Wnt signaling is a master regulator of proliferation and differentiation of intestinal epithelial cells.[7,8] Constitutive activation of this pathway is a hallmark of colorectal cancer.[9–11] Soluble Wnt ligands are secreted by stromal and Paneth cells creating a gradient of Wnt signaling

[1]Group of Biomedical Research in Digestive Tract Tumors, Vall d'Hebron University Hospital Research Institute (VHIR), Universitat Autònoma de Barcelona, 08035 Barcelona, Spain
[2]Group of Molecular Oncology, Biomedical Research Institute of Lleida (IRBLleida), 25198 Lleida, Spain
[3]Instituto de Investigación Biomédica de Salamanca (IBSAL), 37007 Salamanca, Spain
[4]Servicio de Transgénesis, Nucleus, Universidad de Salamanca, 37007 Salamanca, Spain
[5]Departamento de Medicina, Universidad de Salamanca, 37007 Salamanca, Spain
[6]Translational Molecular Pathology, Vall d'Hebron University Hospital Research Institute (VHIR), Universitat Autònoma de Barcelona, 08035 Barcelona, Spain
[7]Centro de Investigación Biomédica en Red de Cáncer (CIBERONC), 28029 Madrid, Spain
[8]Digestive System Research Unit, Vall d'Hebron University Hospital Research Institute (VHIR), 08035 Barcelona, Spain
[9]Department of Chronic Diseases and Metabolism (CHROMETA), Translational Research Center for Gastrointestinal Disorders (TARGID), Leuven 3000, Belgium
[10]Group of Drug Delivery and Targeting, Vall d'Hebron University Hospital Research Institute (VHIR), Universitat Autònoma de Barcelona, 08035 Barcelona, Spain
[11]Clinical Biochemistry Department, Vall d'Hebron University Hospital, 08035 Barcelona, Spain
[12]Department of Biomedical Sciences of Cells and Systems, Section Molecular Cell Biology, University of Groningen, University Medical Center Groningen, Groningen 9713 GZ, the Netherlands
[13]Department of Molecular Genetics, Institute of Biomedical Sciences, Fukushima Medical University School of Medicine, Fukushima 960-1295, Japan
[14]These authors contributed equally
[15]Lead contact
*Correspondence: amartinez@irblleida.cat (Á.M.-B.), darango@irblleida.cat (D.A.)
https://doi.org/10.1016/j.isci.2024.109400

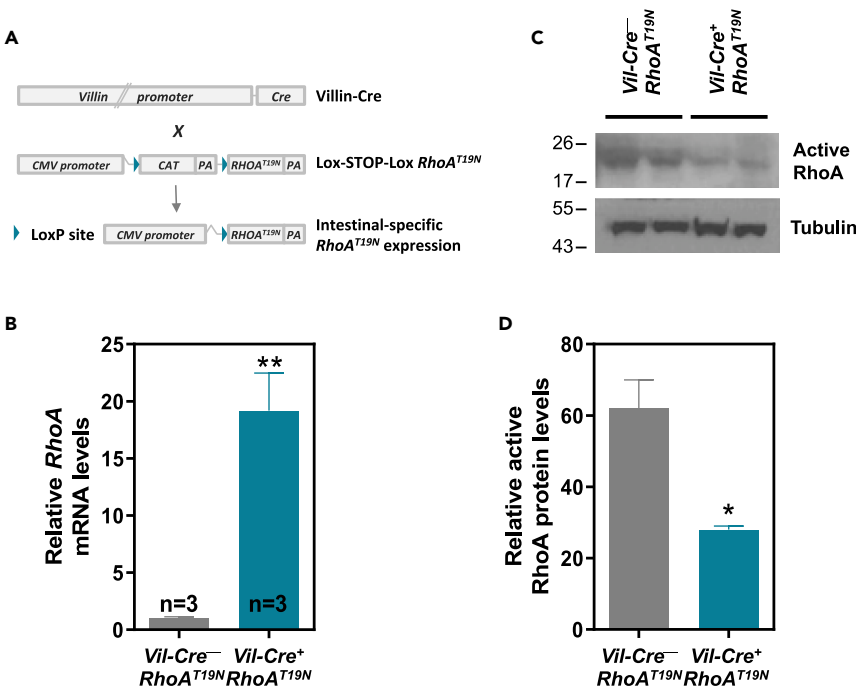

Figure 1. Generation and validation of a mouse model conditionally expressing dominant negative *RhoA*^{T19N}

(A) Lox-STOP-Lox *RhoA*^{T19N} mice were crossed with animals carrying Cre recombinase under the control of the intestine-specific promoter of Villin 1 (*Villin-Cre*). In the double-transgenic mice (*Vil-Cre*$^{+}$*;RhoA*^{T19N}), Cre-loxP recombination deletes the chloramphenicol acetyltransferase (CAT) cassette in the epithelial cells of the intestine, and RhoA^{T19N} is then expressed.

(B) mRNA expression of *RhoA* was assessed by qPCR in the intestine of control mice (*Vil-Cre*$^{-}$*;RhoA*^{T19N}) and animals with intestinal expression of RhoA^{T19N} (*Vil-Cre*$^{+}$*;RhoA*^{T19N}).

(C and D) Relative levels of active (GTP-bound) RhoA were determined in the intestinal epithelium of control (*Vil-Cre*$^{-}$*;RhoA*^{T19N}) and *RhoA*^{T19N} (*Vil-Cre*$^{+}$*;RhoA*^{T19N}) mice using a rhotekin pull-down assay. A representative experiment is shown in (C), and relative levels of GTP-bound active RhoA are quantified in (D). N = number of animals per group. The mean ± SEM is shown. Student's *t* test *p < 0.05; **p < 0.01.

decreasing up the crypt-villus axis.[7,8] In the absence of soluble Wnt ligands, cytoplasmic β-catenin forms a complex with the scaffolding protein Axin, the adenomatous polyposis coli (APC) protein, the E3-ubiquitin ligase β-TrCP, and the kinases glycogen synthase kinase 3β (GSK-3β) and casein kinase 1 (CK1), which can phosphorylate β-catenin and target it for proteasomal degradation.[12,13] The binding of Wnt ligands to the Frizzled transmembrane receptors and LRP5/6 co-receptors leads to the inhibition of the β-catenin destruction complex and the accumulation of cytoplasmic β-catenin that then translocates to the nucleus, binds to transcription factors of the T-cell factor/lymphoid enhancer factor (TCF/LEF) family, and activates the transcription of multiple target genes that regulate proliferation and differentiation of intestinal epithelial cells.[14]

Several members of the Rho family of small GTPases have been shown to be important to maintain the normal function and homeostasis of the intestinal epithelium. Rho proteins act as molecular switches that cycle between a guanosine triphosphate (GTP)-bound active form and a guanosine diphosphate (GDP)-bound inactive form.[15,16] The transition between these two conformational states is regulated through two distinct mechanisms, namely, activation by GTP loading, catalyzed by guanine nucleotide exchange factors (GEFs), and inactivation by GTP hydrolysis, enhanced by GTPase activating proteins (GAPs). In addition, guanosine nucleotide dissociation inhibitors (GDI) sequester Rho GTPases in the cytosol and maintain them in an inactive state. Rho GTPases are the largest family of GTPases comprising more than 22 members.[17] The role in intestinal physiology of two prototypical members of this family, Rac1 and Cdc42, has been characterized using mouse models with targeted inactivation of these proteins. Rac1 is required for expansion of the LGR5 intestinal stem cells, progenitor hyper-proliferation, and cell transformation.[18–20] On the other hand, Cdc42 regulates proliferation, polarity, migration, and differentiation of murine small intestinal epithelial cells.[21] More recently, the short-term effects of the complete ablation of RhoA in the murine intestinal epithelium have been characterized, and a concomitant Wnt signaling downregulation and reduced differentiation and proliferation of intestinal epithelial cells have been reported.[22]

Activation of RhoA signaling has been shown to significantly contribute to the oncogenic process in different types of tumors.[23,24] However, we have previously shown that RhoA has tumor suppressor activity in colorectal cancer.[25,26] Consistently, the loss of this GTPase significantly contributes to tumor progression and metastasis through the activation of canonical Wnt signaling, and reduced RhoA expression is associated with poor prognosis of colorectal cancer patients.[25,26] Moreover, we have reported a complex pattern of inactivation of RhoA in colorectal tumors through genetic losses of chromosome 3p21 affecting the *RHOA* locus, transcriptional regulation through the transforming growth factor β (TGF-β) and Wnt signaling pathways, and post-transcriptional regulation through *miR-200a/b/429*.[27]

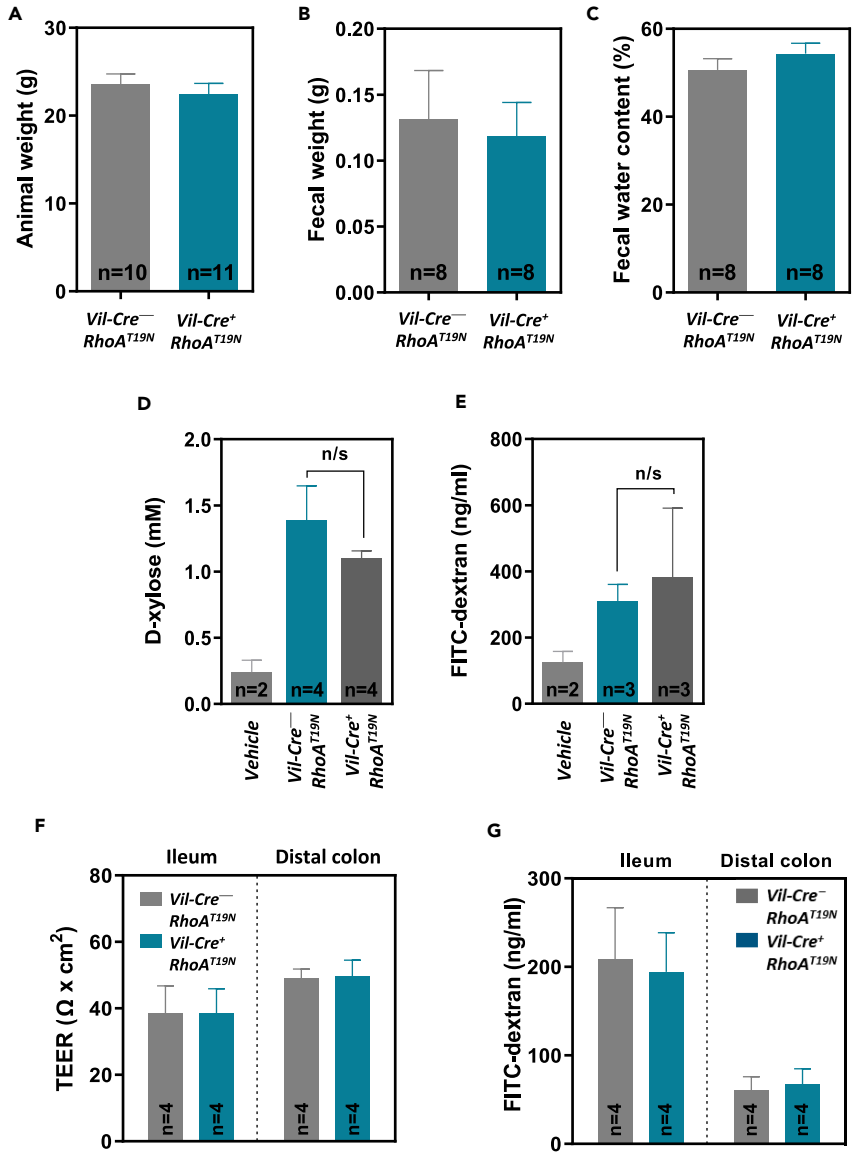

Figure 2. Gross phenotype of mice expressing RhoA^{T19N}

(A) Weight of control (*Vil-Cre;RhoA^{T19N}*) and *RhoA^{T19N}* (*Vil-Cre^{+};RhoA^{T19N}*) mice at 60 days of age.

(B and C) Fecal weight (B) and percentage of water content (C) in 17-month-old control and *RhoA^{T19N}* mice.

(D and E) Transcellular (D) and paracellular (E) epithelial transport and integrity was assessed in *RhoA^{T19N}* and control mice by feeding mice with D-xylose or FITC-dextran, respectively, and determining their presence in plasma 1 or 3 h later, respectively. Background detection levels in control animals that received no D-xylose or FITC-dextran (vehicle) are shown for comparison.

(F) Transepithelial electrical resistance (TEER) of the small and large intestinal mucosa was assessed with the Ussing chamber technique in *RhoA^{T19N}* and control mice.

(G) Epithelial permeability of FITC-dextran was assessed *ex vivo* in the small and large intestinal mucosa of *RhoA^{T19N}* and control mice. N = number of animals per group. The mean ± SEM is shown. n/s, not significant (Student's *t* test $p > 0.05$).

In this study, we investigated the effects of reduced RhoA signaling in the physiology of the small intestinal epithelium. We generated a mouse model with targeted overexpression of a dominant negative form of RhoA (RhoA^{T19N}) in the intestinal epithelium and found that, although mice with RhoA inhibition have no overt defects, their intestinal epithelial cells have shorter microvilli and other differentiation defects. Importantly, we observed elevated Wnt signaling in the normal small intestinal epithelium and higher incidence of intestinal tumors in mice expressing the dominant negative RhoA^{T19N} compared to control animals, indicating that reduced RhoA levels can contribute to intestinal tumor initiation.

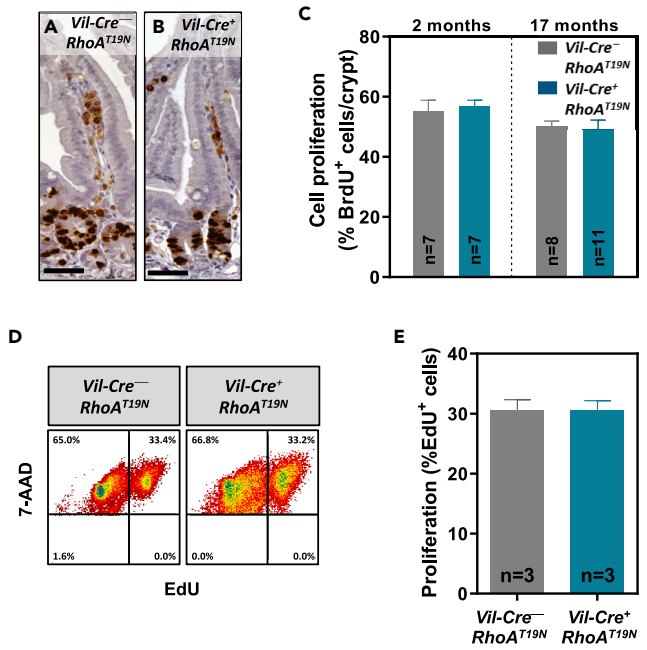

Figure 3. Effects of RhoA inhibition on proliferation of intestinal epithelial cells

(A–D) Two- and 17-month-old mice were intraperitoneally (i.p.) injected with 100 mg/kg 5-Bromo-2′-deoxyuridine (BrdU) 2 h before being euthanized. The number of cells in the S-phase of the cycle during this time was assessed by anti-BrdU immunohistochemistry (A and B; Scale bar: 50 μm). The average number of proliferative cells in the small intestinal epithelium of *RhoA*^{T19N} (*Vil-Cre*$^{+}$;*RhoA*^{T19N}) and control (*Vil-Cre*$^{-}$;*RhoA*^{T19N}) mice at the age of 2 months (C) and 17 months (D) is shown. At least 20 crypts from at least 7 animals per group were scored.

(D and E) The number of proliferating cells in small intestinal organoids derived from *RhoA*^{T19N} and control mice was assessed by flow cytometry after EdU (5-ethynyl-2′-deoxyuridine) staining. Representative results are shown in (D) and the quantification of three independent experiments is shown in (E). N = number of animals per group. The mean ± SEM is shown.

RESULTS

Generation of a mouse model with targeted inhibition of RhoA in the intestinal epithelium

To investigate the role of RhoA in the physiology of the murine intestinal epithelium, we generated a mouse model with a Lox-STOP-Lox cassette upstream of a dominant negative mutant form of this GTPase, RhoA^{T19N} [25,28], that can be expressed upon Cre-Lox recombination. Mice with Cre-dependent expression of RhoA^{T19N} were crossed with animals expressing Cre recombinase under the control of the intestine-specific *Villin 1* promoter (*Vil-Cre*$^{+}$; Figure 1A).[28,29] Cre expression in the small intestinal epithelium of the double-transgenic mice (*Vil-Cre*$^{+}$;*RhoA*^{T19N}) results in the overexpression of the dominant negative RhoA^{T19N} mutant compared to control animals (*Vil-Cre*$^{-}$;*RhoA*^{T19N}; Figure 1B) and a >2-fold reduction in the levels of GTP-bound active RhoA (Figures 1C and 1D).

RhoA inhibition in the intestinal epithelium does not cause an overt phenotype

Mice with (*Vil-Cre*$^{+}$;*RhoA*^{T19N}; n = 52) and without (*Vil-Cre*$^{-}$;*RhoA*^{T19N}; n = 48) intestinal expression of dominant negative *RhoA*^{T19N} were born at the expected Mendelian ratios (Fisher's exact test p = 0.89), and there was no difference in their weight at the age of 60 days (Figure 2A). Moreover, no differences were observed in the weight or water content of the feces of mice with RhoA signaling downregulation compared to control mice (Figures 2B and 2C).

Next, to investigate possible changes after RhoA inhibition in transcellular passive transport and paracellular epithelial permeability, control and *RhoA*^{T19N} mice were orally administered D-xylose and fluorescein isothiocyanate (FITC)-dextran and their plasma concentrations were assessed after 1 or 3 h, respectively.[30,31] No differences were observed in the plasma levels of D-xylose or FITC-dextran in mice with forced expression of dominant negative RhoA^{T19N} compared to control animals (Figures 2D and 2E). Transepithelial electrical resistance (TEER) is commonly used to assess the epithelial barrier function (overall permeability to ions) of the intestinal epithelium.[32] TEER was measured *ex vivo* using freshly dissected mucosal samples from the small and large intestine, and no differences were found in *RhoA*^{T19N} mice compared to control animals (Figure 2F). In addition, using FITC-dextran, no differences were observed in the paracellular permeability of the small and large intestine of *RhoA*^{T19N} mice compared to control animals *ex vivo* (Figure 2G). Collectively, these results indicate that RhoA inhibition in the murine intestine does not cause an overt phenotype and that the normal function of the intestine is maintained.

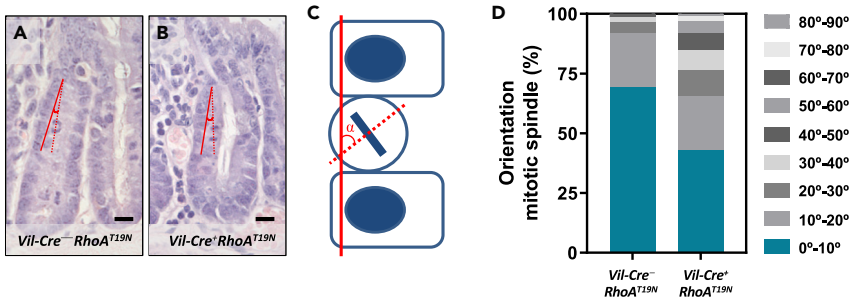

Figure 4. Mitotic spindle orientation in small intestinal epithelial cells

(A–C) The orientation of the mitotic spindle of epithelial cells from the small intestine of control (*Vil-Cre*$^{-}$*;RhoA*^{T19N}; A) and *RhoA*^{T19N} (*Vil-Cre*$^{+}$*;RhoA*^{T19N}; B) mice was determined in hematoxylin and eosin-stained sections by measuring the angle (alpha) formed by the mitotic cell in metaphase or anaphase (dotted red line), and the epithelial surface (solid red line; C). Scale bar: 10 μm.

(D) The percentage of mitotic cells with angles in the indicated intervals is shown for control and *RhoA*^{T19N} mice. At least 140 mitosis were scored in at least 8 animals per group. Fisher's exact test of alpha >30° in control vs. RhoA^{T19N} (5% and 25.2%, respectively), ***p = 1.5 × 10^{-6}.

RhoA and proliferation of intestinal epithelial cells

Intestinal epithelial cells show the fastest rate of proliferation in the adult mouse, and, with the exception of the long-lived Paneth cells and the stem cells, the complete intestinal epithelium is replaced every 4–5 days.[1,33] To investigate the possible effects of reduced RhoA signaling on the proliferation of intestinal epithelial cells, BrdU (5-Bromo-2′-deoxyuridine) was administered to 2- or 17-month-old mice 2 h before being euthanized. Immunohistochemical detection of BrdU incorporated into the DNA during S-phase of the cell cycle in this 2-h window revealed no changes in the number of proliferating cells in the crypts of mice with expression of the dominant negative RhoA^{T19N}, compared to control mice (Figures 3A–3C). Next, intestinal organoids derived from *RhoA*^{T19N} and control animals (n = 3) were cultured *ex vivo* on a three-dimensional Matrigel matrix. To further investigate the possible effects of RhoA downregulation on the proliferation of intestinal epithelial cells, the thymidine analogue EdU (5-ethynyl-2′-deoxyuridine) was added to the growth medium allowing DNA incorporation for 1 h before harvesting the organoids. In good agreement with the *in vivo* findings, fluorescence-activated cell sorting analysis revealed no differences in the number of cells in S-phase in intestinal organoids from *RhoA*^{T19N} and control mice (Figures 3D and 3E). Collectively, these results indicate that downregulation of RhoA signaling does not affect the proliferation of intestinal epithelial cells.

The orientation of cell division is critical for the maintenance of epithelial tissue architecture. In polarized epithelial monolayers, cells normally divide by planar divisions with orientation of the mitotic spindle parallel to the epithelial sheet, and the two daughter cells remain within the same monolayer. RhoA plays a key role in cell division by regulating cytoskeletal reorganization during mitosis, centrosome duplication, and the assembly of the cortical actomyosin network in both the mitotic contractile ring and the cytokinetic furrow.[34–36] Changes in the orientation of the mitotic spindle can lead to asymmetric cell division and thus regulate the positioning, fate, and differentiation of epithelial cells.[37] Changes in RhoA signaling can cause mitotic spindle defects leading to aberrant apico-basal divisions and cell detachment from epithelial sheets.[38–41] Therefore, we next investigated whether downregulation of RhoA signaling in *RhoA*^{T19N} mice affected the orientation of the mitotic spindle of intestinal epithelial cells. Overexpression of RhoA^{T19N} resulted in significant changes in the mitotic spindle orientation. A >5-fold increase was observed in *RhoA*^{T19N} mice compared to control mice in the proportion of dividing cells with a mitotic spindle that deviated more than 30° from the plane of the surface epithelium (Fisher's exact test p = 1.5 × 10^{-6}; Figure 4). These findings suggest that downregulation of RhoA signaling in *RhoA*^{T19N} mice could affect the number of intestinal stem cells as well as the differentiation, maturation, and/or fate of intestinal epithelial cells.

Effects of RhoA inhibition on the stem cell niche

Intestinal stem cells located in the base of the crypts are self-renewing multipotent cells that give rise to all the different cell types found in the mature intestinal epithelium. To investigate possible changes in the number of stem cells in the small intestinal crypts resulting from reduced RhoA signaling, we used immunohistochemical staining of the stem cell marker Olfactomedin 4 (Olfm4).[42] No differences in the number of Olfm4-positive stem cells were found between mice expressing dominant negative RhoA^{T19N} and control animals (Figures 5A and 5B), indicating that reduced RhoA signaling does not have a major impact on the number of intestinal stem cells.

Effects of RhoA inhibition on cell lineage fate

Because other members of the Rho GTPase family have been shown to regulate cell fate and intestinal barrier function in mouse models,[18,21] we next used alkaline phosphatase (AP), Alcian blue, Grimelius' silver staining, and anti-lysozyme immunostaining to identify the four main cell lineages in the small intestinal epithelium, namely, absorptive, goblet, enteroendocrine, or Paneth cells, respectively. No differences were observed in mice with and without expression of RhoA^{T19N} in the localization or the proportion of these different cell types (Figures 5C and S1). Moreover, no differences were observed in the subcellular localization of the apical proteins Ezrin and phospho-ERM and the basolateral proteins Crumbs, E-cadherin, and the transferrin receptor (Figure S2).

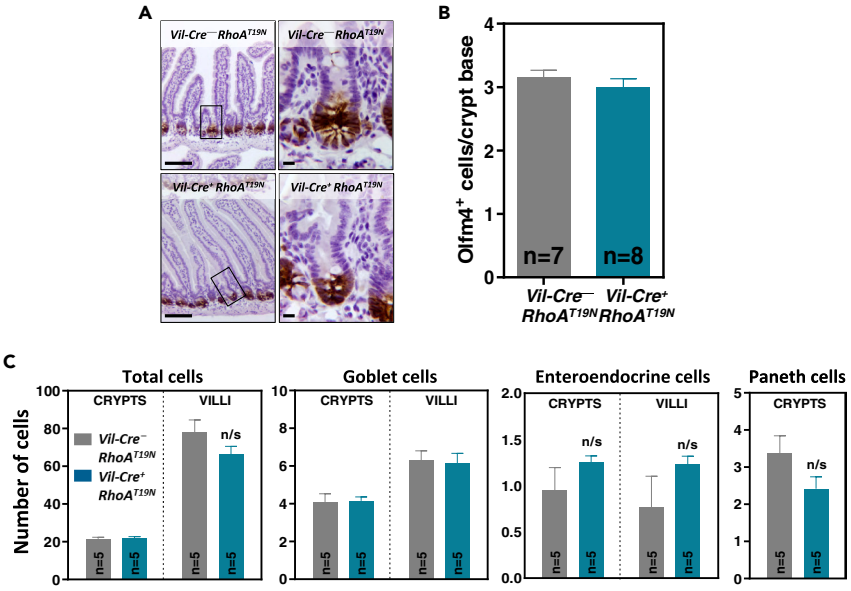

Figure 5. Effects of RhoA inhibition on the histology of intestinal epithelium and barrier function

(A and B) The number of Olfm4^{+} stem cells was determined by immunohistochemistry. Representative results are shown in (A). Scale bars: 50 μm (left) and 5 μm (right). The number of Olfm4^{+} cells located at the base of the crypt (cell positions 0–4) in *RhoA*^{T19N} (*Vil-Cre*$^{+}$;*RhoA*^{T19N}) and control (*Vil-Cre*$^{-}$;*RhoA*^{T19N}) mice was quantified in (B).

(C) The total number of cells (hematoxylin staining) as well as goblet (1% Alcian blue staining), enteroendocrine (Grimelius staining), and Paneth (anti-lysozyme immunostaining) cells were quantified in the villus and crypt compartments of the small intestine of *RhoA*^{T19N} and control mice. N = number of animals per group. The mean ± SEM is shown. n/s: not significant (Student's *t* test $p > 0.05$).

RhoA inhibition causes loss of differentiation and disruption of the brush border

To investigate the role of RhoA in the differentiation of intestinal epithelial cells, we analyzed the levels of activity of three brush border hydrolases that are well-established differentiation markers, namely, dipeptidylpeptidase IV (DPPIV), AP, and sucrose isomaltase (SI). A significant reduction in the activity of DPPIV and AP, but not SI, was observed in the intestinal epithelium of *RhoA*^{T19N} mice compared to control animals (Figures 6A–6C). We next investigated the role of RhoA on the ultrastructure of the brush border of the intestinal epithelial cells using transmission electron microscopy. The epithelium of *RhoA*^{T19N} mice showed widespread microvillus atrophy and reduced microvillus packing compared to control mice, with areas with few/absent microvilli (Figures 6D–6G).

To further investigate the role of RhoA on differentiation, intestinal organoids from *RhoA*^{T19N} and control animals were used. Organoids cultured on a three-dimensional Matrigel matrix differentiate over time and form budding crypt-like structures protruding away from a central cyst.[43,44] In good agreement with the *in vivo* findings, *ex vivo* intestinal organoids from *RhoA*^{T19N} mice showed a significant delay in their differentiation compared to organoids from control mice (Figures 6H–6J). Collectively, these results indicate that RhoA inhibition interferes with the differentiation of intestinal epithelial cells.

RhoA inhibition in the intestinal epithelium activates canonical Wnt signaling

Canonical Wnt/β-catenin signaling is a key regulator of proliferation and differentiation in both normal intestinal epithelial cells and intestinal tumors,[7] and we have reported that the loss of RhoA leads to the accumulation of nuclear β-catenin and enhanced Wnt signaling in colon cancer cells.[25,27] Consistently, immunohistochemical staining revealed increased nuclear β-catenin levels in the small intestinal crypts of *RhoA*^{T19N} mice compared to control animals (Figures 7A and 7B). We therefore investigated whether RhoA regulates canonical Wnt signaling also in normal intestinal cells by assessing possible changes in the expression of a panel of known transcriptional TCF4/β-catenin target genes. A significant increase in the expression of the direct TCF4/β-catenin target genes *c-Myc*, *Cd44*, *Jun*, and *EphB2* was observed in the intestinal epithelium of *RhoA*^{T19N} mice compared to control animals (Figure 7C). As a comparison, we assessed the expression of these TCF4/β-catenin target genes in intestinal tumors from *Apc*^{Min} mice[45] and found that, as expected, *Apc* mutations result in a more robust Wnt activation than RhoA signaling downregulation (Figure 7C). Moreover, these findings were further confirmed using intestinal organoids derived from the normal intestine of either *RhoA*^{T19N} or control mice and intestinal tumors from *Apc*^{Min} mice (Figure 7D). Collectively, these results indicate that downregulation of RhoA signaling leads to increased nuclear β-catenin and causes chronic Wnt activation in intestinal epithelial cells, although the magnitude is lower than the enhanced Wnt signaling observed in fully blown intestinal adenomas carrying *Apc* mutations.

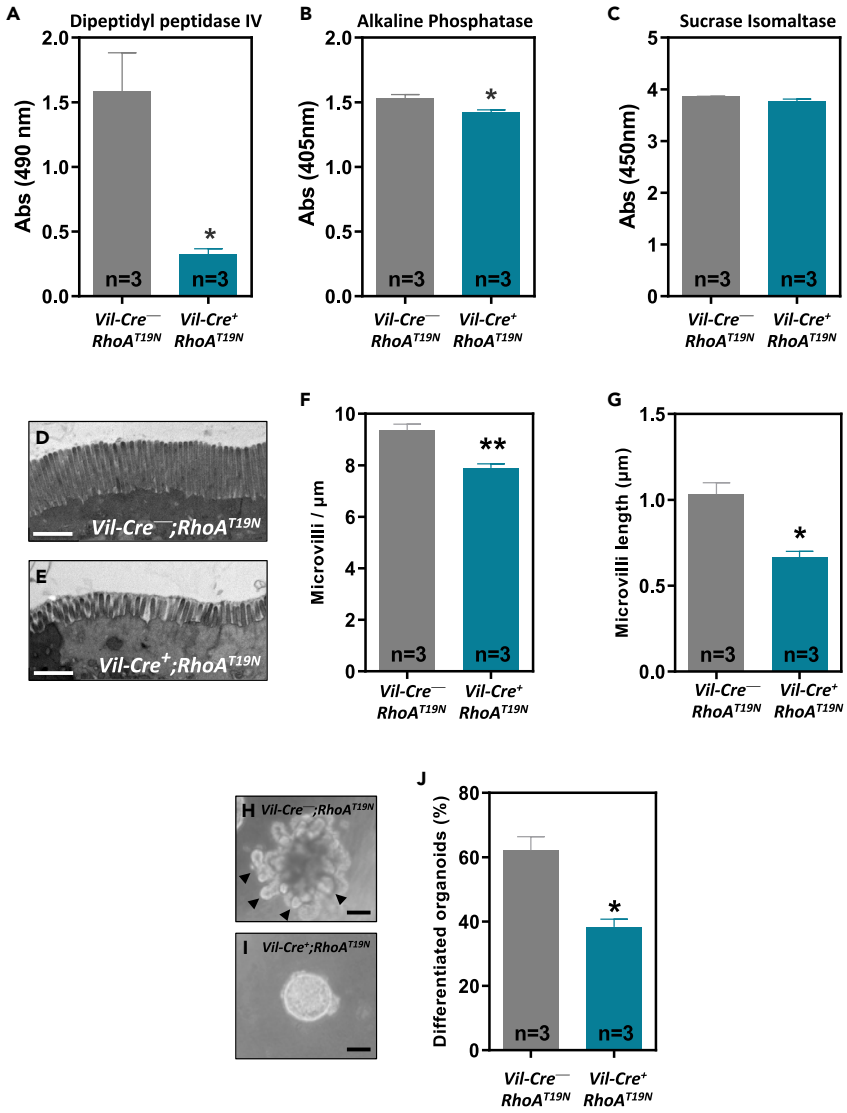

Figure 6. Effects of RhoA inhibition on enterocyte differentiation and brush border formation

(A–C) The activity of the brush border enzymes dipeptidylpeptidase IV (A), alkaline phosphatase (B), and sucrose isomaltase (C) was determined in the normal intestine of 13-week-old *RhoA*^{T19N} (*Vil-Cre*$^{+}$;*RhoA*^{T19N}) and control (*Vil-Cre*$^{-}$;*RhoA*^{T19N}).

(D and E) Representative transmission electron microscopy pictures of the brush border of epithelial absorptive cells from the small intestine of 13-week-old control mice (D) and *RhoA*^{T19N} animals (E). Scale bar: 1 µm.

(F and G) show the average density and length of the microvilli of *RhoA*^{T19N} and control mice.

(H and I) Representative photos of duodenal organoids derived from control (H) or *RhoA*^{T19N} (I) mice. Arrowheads indicate budding crypt-like structures in differentiated organoids. Scale bar: 50 µm.

(J) Percentage of differentiated organoids (i.e., showing budding crypt-like structures) derived from *RhoA*^{T19N} and control mice at the indicated times after seeding in 3D Matrigel cultures. N = number of animals per group. The mean ± SEM is shown. Student's *t* test *p < 0.05; **p < 0.01.

RhoA regulates the differentiation of intestinal epithelial cells through Wnt signaling

Canonical Wnt/β-catenin signaling is known to be a master regulator of differentiation of intestinal epithelial cells.[7,8] To investigate whether the effects of RhoA on the differentiation of intestinal epithelial cells were due to the observed changes in Wnt signaling in *RhoA*^{T19N} mice, we used the Wnt inhibitor IWR-1-endo[46] to block the enhancement of Wnt signaling resulting from RhoA downregulation in intestinal organoids. Dose titration of IWR-1-endo determined that a concentration of 200 nM prevented the increased Wnt signaling observed in organoids from *RhoA*^{T19N} mice compared to control animals (Figures 8A and S3), and this treatment completely restored the capacity of intestinal organoids to differentiate in these culture conditions (Figures 8B and 8C). These results demonstrate that the reduced differentiation of intestinal epithelial cells resulting from RhoA inhibition is fully dependent on Wnt/β-catenin signaling.

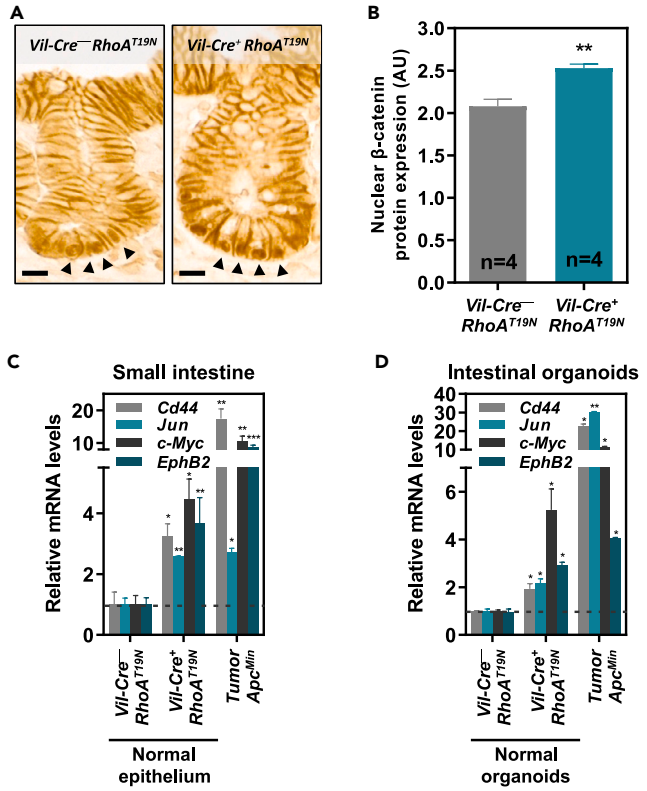

Figure 7. Effects of RhoA downregulation on Wnt signaling

(A and B) β-catenin levels were assessed by immunohistochemistry in the small intestinal epithelium of *RhoA*^{T19N} and control mice (A), and the intensity of all positive nuclei in crypts cells was quantified (B). Arrowheads indicate representative positive cells for nuclear β-catenin staining. Scale bar: 10 μm. N = number of animals per group.

(C and D) The expression of the Wnt target genes *Cd44*, *Jun*, *c-Myc*, and *EphB2* was assessed by qPCR in the intestinal epithelium (duodenum) of 13-week-old *RhoA*^{T19N} (*Vil-Cre*$^{+}$*;RhoA*^{T19N}) and control (*Vil-Cre*$^{-}$*;RhoA*^{T19N}) mice (C), and small intestinal organoids derived from these animals (D). The effects of *Apc* inactivation on Wnt signaling target genes in intestinal tumors of *Apc*^{Min} mice (C) and organoids derived from these tumors (D) are shown for comparison. Mean expression ±SEM in the normal epithelium of three animals or three experiments with intestinal organoids is shown. Student's *t* test *p < 0.05; **p < 0.01; ***p < 0.001.

Reduced RhoA signaling results in increased intestinal tumorigenesis

We have previously shown that RhoA inactivation using the T19N dominant negative mutant of RhoA significantly accelerates the progression of intestinal tumors initiated genetically (*Apc*^{Min} mice) or pharmacologically (azoxymethane; AOM).[25] However, the role of RhoA in the initiation of intestinal tumorigenesis has not been directly studied. Here, we first investigated the effects of intestinal RhoA inhibition in *RhoA*^{T19N} mice on their lifespan and found no significant differences when compared to *Vil-Cre*$^{-}$*;RhoA*^{T19N} control mice (Figure 9A). Next, to directly investigate the role of RhoA in tumor initiation, 17-month-old control and *RhoA*^{T19N} mice were euthanized and the number of macroscopically visible tumors scored. Six of the nine (66.7%) mice expressing *RhoA*^{T19N} had tumors in their small intestine, compared to two out of ten (20%) control mice (Figure 9B; Fisher's exact test, p = 0.03). Moreover, although the average size of their intestinal tumors was not significantly different (Figure 9C), inhibition of RhoA significantly increased the multiplicity of lesions in tumor-bearing *RhoA*^{T19N} mice compared to control animals (Figure 9B). Hematoxylin and eosin staining of sections of formalin-fixed, paraffin-embedded intestinal samples confirmed the presence of intestinal tumors (Figures 9D and 9E). Collectively, these results indicate that the inhibition of RhoA in the normal murine intestine is sufficient to initiate the tumorigenic process.

DISCUSSION

GTPases of the Rho family are key regulators of multiple cellular processes such as motility, adhesion, differentiation, polarization, and proliferation.[15,23,47,48] Our understanding of the role of these GTPases in the normal and pathological function of the intestinal epithelium largely relies on the use of cell culture systems, most often using colon cancer cell lines, like CACO2, T84, or HT29.[15] The capacity to edit the mouse genome allows now investigation of the role of GTPases in intestinal homeostasis and maintenance of barrier function *in vivo*. Targeted inactivation of the related Cdc42 GTPase in the murine intestine has been reported to result in a significant reduction of their body weight and

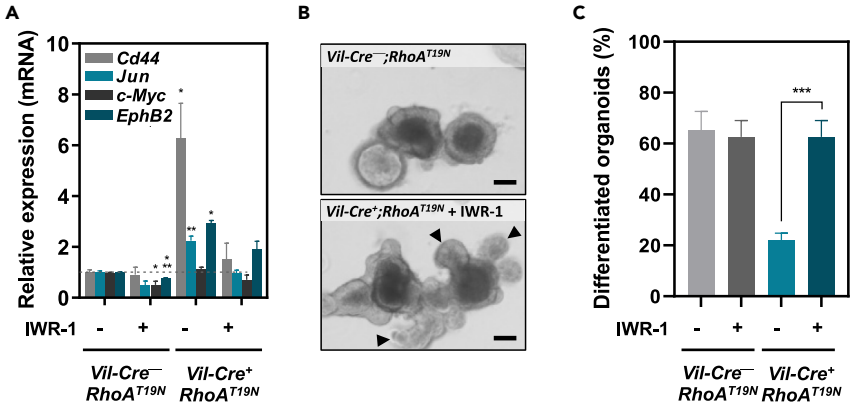

Figure 8. Effects of the inhibition of RhoA^{T19N}-dependent Wnt activation

(A) Relative levels of expression of the Wnt target genes *Cd44*, *Jun*, *c-Myc*, and *EphB2* after treatment with the Wnt inhibitor IWR-1-endo (200 nM) in small intestinal organoids derived from *RhoA^{T19N}* (*Vil-Cre^{+};RhoA^{T19N}*) and control (*Vil-Cre^{-};RhoA^{T19N}*) mice.

(B and C) Effects of IWR-1-mediated Wnt inhibition on the differentiation of organoids derived from the small intestine of *RhoA^{T19N}* and control mice. Representative photos of duodenal organoids derived from *RhoA^{T19N}* in the presence or absence of IWR-1 treatment (B). Arrowheads indicate budding crypt-like structures in differentiated organoids. Scale bar: 50 μm. The mean percentage of differentiated organoids from *RhoA^{T19N}* and control mice is shown in panel (C). The mean ± SEM in three independent experiments each of them carried out in triplicate is shown. Student's *t* test *p < 0.05; ***p < 0.001.

shorter lifespan associated with defects in the regulation of proliferation and differentiation of the intestinal epithelium.[21] Moreover, inactivation of Rac1 in the murine intestine was found to cause intestinal barrier breakdown.[18]

To investigate the role of RhoA in intestinal physiology, here we used a mouse model that allows Cre-dependent overexpression of the thoroughly characterized T19N dominant negative mutant form of RhoA.[28,49–51] The resulting >2-fold reduction in the levels of GTP-bound active RhoA did not cause any changes in animal weight, fecal water content, the histology of the small intestine, intestinal barrier function, or animal survival, indicating that intestinal function is not significantly altered. Although RhoA^{T19N} overexpression has the potential to interfere with signaling pathways regulated by other GTPases that share common GEFs with RhoA, there is a large body of literature using this tool and the effects observed with RhoA^{T19N} are remarkably specific.[52,53] For example, RhoA^{T19N} or short hairpin RNA (shRNA)-mediated RHOA signaling downregulation have been shown to cause the same phenotype in human embryonic stem cells, which is different from the phenotype observed with RHOB or RHOC dominant negative proteins.[54] Moreover, we have reported that RhoA^{T19N} overexpression precisely phenocopies the effects of RhoA knockdown by RNA interference in colon cancer cells.[25]

As observed before in colon cancer cells,[25] reduced Rho signaling leads to elevated nuclear levels of the transcriptional activator β-catenin in mouse epithelial cells residing at the bottom of intestinal crypts. Consistently, we found that RhoA inactivation in intestinal epithelial cells resulted in a significant elevation of the expression of multiple β-catenin/TCF4 target genes in the normal intestinal mucosa and intestinal organoids. Canonical Wnt/β-catenin signaling is a key regulator of proliferation and differentiation of normal intestinal epithelial cells. Indeed, aberrant activation of Wnt signaling, mostly through mutations in *APC* or other members of the β-catenin destruction complex, constitutes the initiating event of the vast majority of colorectal tumors.[9–11] Mouse models of targeted inactivation of *Apc* in normal intestinal epithelial cells demonstrate a robust activation of Wnt signaling that leads to a concomitant increase in proliferation and inhibition of differentiation.[55,56] Consistently, we have shown that RhoA downregulation in human colon cancer cells results in a significant elevation of Wnt signaling that leads to increased proliferation and reduced differentiation of intestinal tumor cells.[25]

Here, we found that elevated Wnt/β-catenin signaling in the normal intestinal mucosa of *RhoA^{T19N}* mice was associated with reduced differentiation of the intestinal epithelium, as revealed by reduced number/length of apical microvilli, lower levels of activity of some enterocytic markers, and inhibition of the formation of crypt-like branching structures in intestinal organoid cultures. Importantly, we show that the reduced differentiation observed in intestinal organoid cultures is strictly dependent on the elevated Wnt signaling resulting from reduced RhoA signaling, as indicated by Wnt inhibition with the IWR-1 inhibitor in the organoids derived from RhoA^{T19N} mice. These results are consistent with earlier findings showing that RhoA is important for the differentiation of intestinal tumor cells upon vitamin D treatment, LKB1 induction, or spontaneous differentiation of confluent cultures.[25,57] However, although intestinal RhoA inactivation resulted in increased rates of tumor initiation, no proliferative changes were observed in the normal intestinal epithelium. Interestingly, the enhanced Wnt signaling observed in normal epithelial cells after RhoA inhibition is significantly lower than the Wnt activation found in intestinal tumors due to *Apc* mutations. This suggests that higher levels of Wnt signaling are required for the mitogenic effects of Wnt than for the inhibition of differentiation of intestinal epithelial cells. Strikingly, however, Lui et al. have recently shown that complete inactivation of RhoA in the murine intestinal epithelium results in reduced Wnt signaling and inhibition of proliferation, and causes a severe disruption of the crypt-villus architecture within the first 5 days after RhoA ablation.[22] However, although most of these intestine-specific RhoA knockout mice survived and recovered from the effects of acute RhoA ablation, the long-term effects of complete RhoA inactivation on Wnt signaling and the histology of the intestine were not investigated in the surviving RhoA knockout mice.[22]

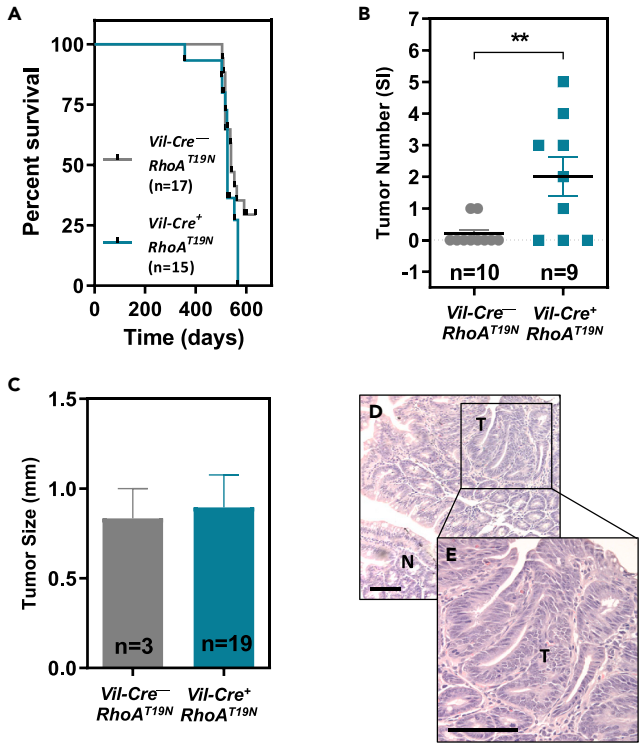

Figure 9. Effects of RhoA inhibition on intestinal tumorigenesis

(A) Kaplan-Meier curves showing the survival of *RhoA*^{T19N} (*Vil-Cre*$^{+}$;*RhoA*^{T19N}) and control (*Vil-Cre*$^{-}$;*RhoA*^{T19N}) mice (Log -rank test p = 0.22).

(B) Total number of macroscopically visible tumors in the small intestine of 17-month-old *RhoA*^{T19N} and control mice. N = number of animals per group.

(C) Average size of tumors in the small intestine of *RhoA*^{T19N} and control mice. N = number of tumors included in the analysis.

(D) Micrograph showing the normal small intestinal mucosa (N) and a representative intestinal tumor (T) in a *RhoA*^{T19N} mouse.

(E) The indicated region is shown at higher magnification. Scale bar: 100 μm. The mean ± SEM is shown. Student's *t* test **p < 0.01.

Importantly, although several genes have been shown to accelerate the oncogenic process after genetic- or carcinogen-initiated tumorigenesis, few genes have been reported to be able to initiate the tumorigenic process after their inactivation in the murine intestinal epithelium. Mutations in the tumor suppressor gene *Apc* have long been known to efficiently initiate the tumorigenic process in both the human and murine intestine.[45,58,59] Inactivation of other genes such as Cdx2,[60] Msh2,[61] or Msh6[62] has been shown to lead to tumor formation in the gastrointestinal tract of mice. We report here that RhoA inhibition in the intestinal epithelium is sufficient to cause a significant increase in the incidence of intestinal tumors, demonstrating the importance of RhoA signaling as a suppressor of tumor initiation and progression in this organ.[25,26]

The undifferentiated state of cancer cells is widely believed to be the result of the abnormal continuous division of these cells, and it is currently not well understood to what extent the loss of differentiation can prime epithelial cells for malignant transformation. Studies in Drosophila have demonstrated that inactivation of genes involved in epithelial cell polarity is an important step during early tumorigenesis.[63–66] Moreover, both RhoA[38,67] and heterozygous *Apc* mutations[68–70] have been reported to regulate planar spindle orientation during the asymmetric division characteristic of stem cells, which might contribute to intestinal tumor initiation without increasing proliferation, although the contribution of canonical Wnt signaling to these effects remains to be elucidated.

In summary, we report here that inhibition of RhoA signaling in the murine intestine leads to nuclear β-catenin accumulation, increased Wnt signaling, loss of differentiation, and increased number of intestinal tumors. These results indicate that RhoA is important for maintaining the normal physiology of the intestinal epithelium and reveal a new tumor suppressor function for RhoA in the gastrointestinal tract.

Limitations of the study

While our study sheds light on the crucial role of RhoA in the regulation of intestinal cell differentiation and tumor initiation through Wnt signaling, certain limitations should be acknowledged. The investigation relies on a mouse model with conditional overexpression of a dominant negative RhoA mutant, which may not fully recapitulate the complexities of human intestinal physiology. In addition, the study primarily explores the Wnt pathway, and a broader exploration of additional factors and pathways controlling intestinal homeostasis could provide a more comprehensive understanding of the intricate regulatory mechanisms involved.

STAR★METHODS

Detailed methods are provided in the online version of this paper and include the following:

SUPPLEMENTAL INFORMATION

Supplemental information can be found online at https://doi.org/10.1016/j.isci.2024.109400.

ACKNOWLEDGMENTS

This work was supported by the IRBLleida Immunohistochemistry and Histology Core Facility.

This study was partially funded by grants of Instituto de Salud Carlos III (ISCIII) and co-funded by the European Union (PI19/00993, PI22/00773), European Regional Development Funds (AC19/00095-EuroNanoMed III, AC20/00022-European Joint Program for Rare Diseases), and the Spanish Association Against Cancer (AECC GCA15152966ARAN) to D.A. and grants of Instituto de Salud Carlos III (ISCIII), the European Union (PI23/01062), and Diputació de Lleida (PIRS21/03) to A.M.-B.

AUTHOR CONTRIBUTIONS

Study concept and design: D.A., H.D., and P.R. Acquisition of data: H.D., P.R., F.C.-G., I.M., J.B., E.A., L.J., B.B., N.V., L.B., M.V., M.S.-M., S.L., S.R.y.C., R.N., R.F., S.S.J., S.C.D.v.I., K.K., and A.M.-B. Analysis and interpretation of data: D.A., H.D., P.R., and A.M.-B. Drafting of the manuscript: D.A., H.D., P.R., and A.M.-B. All authors have read and approved the final version of the manuscript.

DECLARATION OF INTERESTS

The authors declare no competing interests.

Received: April 26, 2023
Revised: December 23, 2023
Accepted: February 28, 2024
Published: March 1, 2024

REFERENCES

1. Cheng, H., and Leblond, C.P. (1974). Origin, differentiation and renewal of the four main epithelial cell types in the mouse small intestine. V. Unitarian Theory of the origin of the four epithelial cell types. Am. J. Anat. *141*, 537–561. https://doi.org/10.1002/aja.1001410407.
2. Clevers, H. (2013). The intestinal crypt, a prototype stem cell compartment. Cell *154*, 274–284. https://doi.org/10.1016/j.cell.2013.07.004.
3. Cheng, H., and Leblond, C.P. (1974). Origin, differentiation and renewal of the four main epithelial cell types in the mouse small intestine. I. Columnar cell. Am. J. Anat. *141*, 461–479. https://doi.org/10.1002/aja.1001410403.
4. Cheng, H. (1974). Origin, differentiation and renewal of the four main epithelial cell types in the mouse small intestine. II. Mucous cells. Am. J. Anat. *141*, 481–501. https://doi.org/10.1002/aja.1001410404.
5. Cheng, H., and Leblond, C.P. (1974). Origin, differentiation and renewal of the four main epithelial cell types in the mouse small intestine. III. Entero-endocrine cells. Am. J. Anat. *141*, 503–519. https://doi.org/10.1002/aja.1001410405.
6. Cheng, H. (1974). Origin, differentiation and renewal of the four main epithelial cell types in the mouse small intestine. IV. Paneth cells. Am. J. Anat. *141*, 521–535. https://doi.org/10.1002/aja.1001410406.
7. MacDonald, B.T., Tamai, K., and He, X. (2009). Wnt/beta-catenin signaling: components, mechanisms, and diseases. Dev. Cell *17*, 9–26. https://doi.org/10.1016/j.devcel.2009.06.016.
8. Clevers, H. (2006). Wnt/beta-catenin signaling in development and disease. Cell *127*, 469–480. https://doi.org/10.1016/j.cell.2006.10.018.
9. Bienz, M., and Clevers, H. (2000). Linking colorectal cancer to Wnt signaling. Cell *103*, 311–320. https://doi.org/10.1016/s0092-8674(00)00122-7.
10. Polakis, P. (2000). Wnt signaling and cancer. Genes Dev. *14*, 1837–1851. https://doi.org/10.1101/gad.14.15.1837.
11. Morin, P.J., Sparks, A.B., Korinek, V., Barker, N., Clevers, H., Vogelstein, B., and Kinzler, K.W. (1997). Activation of beta-catenin-Tcf signaling in colon cancer by mutations in beta-catenin or APC. Science *275*, 1787–1790. https://doi.org/10.1126/science.275.5307.1787.
12. Behrens, J., von Kries, J.P., Kühl, M., Bruhn, L., Wedlich, D., Grosschedl, R., and Birchmeier, W. (1996). Functional interaction of beta-catenin with the transcription factor LEF-1. Nature *382*, 638–642. https://doi.org/10.1038/382638a0.
13. Molenaar, M., van de Wetering, M., Oosterwegel, M., Peterson-Maduro, J., Godsave, S., Korinek, V., Roose, J., Destrée, O., and Clevers, H. (1996). XTcf-3 transcription factor mediates beta-catenin-induced axis formation in Xenopus embryos. Cell *86*, 391–399. https://doi.org/10.1016/s0092-8674(00)80112-9.
14. Reya, T., and Clevers, H. (2005). Wnt signalling in stem cells and cancer. Nature *434*, 843–850. https://doi.org/10.1038/nature03319.
15. Leve, F., and Morgado-Díaz, J.A. (2012). Rho GTPase signaling in the development of colorectal cancer. J. Cell. Biochem. *113*, 2549–2559. https://doi.org/10.1002/jcb.24153.
16. Hodge, R.G., and Ridley, A.J. (2016). Regulating Rho GTPases and their regulators. Nat. Rev. Mol. Cell Biol. *17*, 496–510. https://doi.org/10.1038/nrm.2016.67.
17. Ridley, A.J. (2006). Rho GTPases and actin dynamics in membrane protrusions and vesicle trafficking. Trends Cell Biol. *16*, 522–529. https://doi.org/10.1016/j.tcb.2006.08.006.
18. Myant, K.B., Cammareri, P., McGhee, E.J., Ridgway, R.A., Huels, D.J., Cordero, J.B., Schwitalla, S., Kalna, G., Ogg, E.-L., Athineos, D., et al. (2013). ROS production and NF-κB activation triggered by RAC1 facilitate WNT-driven intestinal stem cell proliferation and colorectal cancer initiation. Cell Stem Cell *12*, 761–773. https://doi.org/10.1016/j.stem.2013.04.006.
19. Stappenbeck, T.S., and Gordon, J.I. (2000). Rac1 mutations produce aberrant epithelial differentiation in the developing and adult mouse small intestine. Development *127*, 2629–2642. https://doi.org/10.1242/dev.127.12.2629.
20. Myant, K.B., Scopelliti, A., Haque, S., Vidal, M., Sansom, O.J., and Cordero, J.B. (2013). Rac1 drives intestinal stem cell proliferation and regeneration. Cell Cycle *12*, 2973–2977. https://doi.org/10.4161/cc.26031.
21. Melendez, J., Liu, M., Sampson, L., Akunuru, S., Han, X., Vallance, J., Witte, D., Shroyer, N., and Zheng, Y. (2013). Cdc42 coordinates proliferation, polarity, migration, and differentiation of small intestinal epithelial cells in mice. Gastroenterology *145*, 808–819. https://doi.org/10.1053/j.gastro.2013.06.021.
22. Liu, M., Zhang, Z., Sampson, L., Zhou, X., Nalapareddy, K., Feng, Y., Akunuru, S., Melendez, J., Davis, A.K., Bi, F., et al. (2017). RHOA GTPase Controls YAP-Mediated EREG Signaling in Small Intestinal Stem Cell Maintenance. Stem Cell Rep. *9*, 1961–1975. https://doi.org/10.1016/j.stemcr.2017.10.004.
23. Sahai, E., and Marshall, C.J. (2002). RHO-GTPases and cancer. Nat. Rev. Cancer *2*, 133–142. https://doi.org/10.1038/nrc725.
24. Pradhan, R., Ngo, P.A., Martínez-Sánchez, L.D., Neurath, M.F., and López-Posadas, R. (2021). Rho GTPases as Key Molecular Players within Intestinal Mucosa and GI Diseases. Cells *10*. https://doi.org/10.3390/cells10010066.
25. Rodrigues, P., Macaya, I., Bazzocco, S., Mazzolini, R., Andretta, E., Dopeso, H., Mateo-Lozano, S., Bilić, J., Cartón-García, F., Nieto, R., et al. (2014). RHOA inactivation enhances Wnt signalling and promotes colorectal cancer. Nat. Commun. *5*, 5458. https://doi.org/10.1038/ncomms6458.
26. Arango, D., Laiho, P., Kokko, A., Alhopuro, P., Sammalkorpi, H., Salovaara, R., Nicorici, D., Hautaniemi, S., Alazzouzi, H., Mecklin, J.-P., et al. (2005). Gene-expression profiling predicts recurrence in Dukes' C colorectal cancer. Gastroenterology *129*, 874–884. https://doi.org/10.1053/j.gastro.2005.06.066.
27. Dopeso, H., Rodrigues, P., Bilic, J., Bazzocco, S., Cartón-García, F., Macaya, I., de Marcondes, P.G., Anguita, E., Masanas, M., Jiménez-Flores, L.M., et al. (2018). Mechanisms of inactivation of the tumour suppressor gene RHOA in colorectal cancer. Br. J. Cancer *118*, 106–116. https://doi.org/10.1038/bjc.2017.420.
28. Kobayashi, K., Takahashi, M., Matsushita, N., Miyazaki, J.i., Koike, M., Yaginuma, H., Osumi, N., Kaibuchi, K., and Kobayashi, K. (2004). Survival of developing motor neurons mediated by Rho GTPase signaling pathway through Rho-kinase. J. Neurosci. *24*, 3480–3488. https://doi.org/10.1523/JNEUROSCI.0295-04.2004.
29. Madison, B.B., Dunbar, L., Qiao, X.T., Braunstein, K., Braunstein, E., and Gumucio, D.L. (2002). Cis elements of the villin gene control expression in restricted domains of the vertical (crypt) and horizontal (duodenum, cecum) axes of the intestine. J. Biol. Chem. *277*, 33275–33283. https://doi.org/10.1074/jbc.M204935200.
30. Goodwin, M.A., Nersessian, B.N., Brown, J., and Fletcher, O.J. (1985). Gastrointestinal transit times in normal and reovirus-inoculated turkeys. Avian Dis. *29*, 920–928. https://doi.org/10.2307/1590445.
31. Anderson, J.M., Balda, M.S., and Fanning, A.S. (1993). The structure and regulation of tight junctions. Curr. Opin. Cell Biol. *5*, 772–778. https://doi.org/10.1016/0955-0674(93)90024-k.
32. Gitter, A.H., Fromm, M., and Schulzke, J.D. (1998). Impedance analysis for the determination of epithelial and subepithelial resistance in intestinal tissues. J. Biochem. Biophys. Methods *37*, 35–46. https://doi.org/10.1016/s0165-022x(98)00016-5.
33. Barker, N. (2014). Adult intestinal stem cells: critical drivers of epithelial homeostasis and regeneration. Nat. Rev. Mol. Cell Biol. *15*, 19–33. https://doi.org/10.1038/nrm3721.
34. Chircop, M. (2014). Rho GTPases as regulators of mitosis and cytokinesis in mammalian cells. Small GTPases *5*, e29770. https://doi.org/10.4161/sgtp.29770.
35. Kanai, M., Crowe, M.S., Zheng, Y., Vande Woude, G.F., and Fukasawa, K. (2010). RhoA and RhoC are both required for the ROCK II-dependent promotion of centrosome duplication. Oncogene *29*, 6040–6050. https://doi.org/10.1038/onc.2010.328.
36. Basant, A., and Glotzer, M. (2018). Spatiotemporal Regulation of RhoA during Cytokinesis. Curr. Biol. *28*, R570–R580. https://doi.org/10.1016/j.cub.2018.03.045.
37. Donà, F., Eli, S., and Mapelli, M. (2022). Insights Into Mechanisms of Oriented Division From Studies in 3D Cellular Models. Front. Cell Dev. Biol. *10*, 847801. https://doi.org/10.3389/fcell.2022.847801.
38. Roszko, I., Afonso, C., Henrique, D., and Mathis, L. (2006). Key role played by RhoA in the balance between planar and apico-basal cell divisions in the chick neuroepithelium. Dev. Biol. *298*, 212–224. https://doi.org/10.1016/j.ydbio.2006.06.031.
39. Bakal, C.J., Finan, D., LaRose, J., Wells, C.D., Gish, G., Kulkarni, S., DeSepulveda, P., Wilde, A., and Rottapel, R. (2005). The Rho GTP exchange factor Lfc promotes spindle assembly in early mitosis. Proc. Natl. Acad. Sci. USA *102*, 9529–9534. https://doi.org/10.1073/pnas.0504190102.
40. Aoki, T., Ueda, S., Kataoka, T., and Satoh, T. (2009). Regulation of mitotic spindle formation by the RhoA guanine nucleotide exchange factor ARHGEF10. BMC Cell Biol. *10*, 56. https://doi.org/10.1186/1471-2121-10-56.

41. Vasiliev, J.M., Omelchenko, T., Gelfand, I.M., Feder, H.H., and Bonder, E.M. (2004). Rho overexpression leads to mitosis-associated detachment of cells from epithelial sheets: a link to the mechanism of cancer dissemination. Proc. Natl. Acad. Sci. USA *101*, 12526–12530. https://doi.org/10.1073/pnas.0404723101.
42. van der Flier, L.G., Haegebarth, A., Stange, D.E., van de Wetering, M., and Clevers, H. (2009). OLFM4 is a robust marker for stem cells in human intestine and marks a subset of colorectal cancer cells. Gastroenterology *137*, 15–17. https://doi.org/10.1053/j.gastro.2009.05.035.
43. Sato, T., Vries, R.G., Snippert, H.J., van de Wetering, M., Barker, N., Stange, D.E., van Es, J.H., Abo, A., Kujala, P., Peters, P.J., and Clevers, H. (2009). Single Lgr5 stem cells build crypt-villus structures *in vitro* without a mesenchymal niche. Nature *459*, 262–265. https://doi.org/10.1038/nature07935.
44. Sato, T., and Clevers, H. (2013). Growing self-organizing mini-guts from a single intestinal stem cell: mechanism and applications. Science *340*, 1190–1194. https://doi.org/10.1126/science.1234852.
45. Moser, A.R., Pitot, H.C., and Dove, W.F. (1990). A dominant mutation that predisposes to multiple intestinal neoplasia in the mouse. Science *247*, 322–324. https://doi.org/10.1126/science.2296722.
46. Chen, B., Dodge, M.E., Tang, W., Lu, J., Ma, Z., Fan, C.-W., Wei, S., Hao, W., Kilgore, J., Williams, N.S., et al. (2009). Small molecule-mediated disruption of Wnt-dependent signaling in tissue regeneration and cancer. Nat. Chem. Biol. *5*, 100–107. https://doi.org/10.1038/nchembio.137.
47. Citalán-Madrid, A.F., García-Ponce, A., Vargas-Robles, H., Betanzos, A., and Schnoor, M. (2013). Small GTPases of the Ras superfamily regulate intestinal epithelial homeostasis and barrier function via common and unique mechanisms. Tissue Barriers *1*, e26938. https://doi.org/10.4161/tisb.26938.
48. Jaffe, A.B., and Hall, A. (2005). Rho GTPases: biochemistry and biology. Annu. Rev. Cell Dev. Biol. *21*, 247–269. https://doi.org/10.1146/annurev.cellbio.21.020604.150721.
49. Sahai, E., Alberts, A.S., and Treisman, R. (1998). RhoA effector mutants reveal distinct effector pathways for cytoskeletal reorganization, SRF activation and transformation. EMBO J. *17*, 1350–1361. https://doi.org/10.1093/emboj/17.5.1350.
50. Nguyen, Q.-D., De Wever, O., Bruyneel, E., Hendrix, A., Xie, W.-Z., Lombet, A., Leibl, M., Mareel, M., Gieseler, F., Bracke, M., and Gespach, C. (2005). Commutators of PAR-1 signaling in cancer cell invasion reveal an essential role of the Rho-Rho kinase axis and tumor microenvironment. Oncogene *24*, 8240–8251. https://doi.org/10.1038/sj.onc.1208990.
51. Bruewer, M., Hopkins, A.M., Hobert, M.E., Nusrat, A., and Madara, J.L. (2004). RhoA, Rac1, and Cdc42 exert distinct effects on epithelial barrier via selective structural and biochemical modulation of junctional proteins and F-actin. Am. J. Physiol. Cell Physiol. *287*, C327–C335. https://doi.org/10.1152/ajpcell.00087.2004.
52. Schaefer, A., Reinhard, N.R., and Hordijk, P.L. (2014). Toward understanding RhoGTPase specificity: structure, function and local activation. Small GTPases *5*, 6. https://doi.org/10.4161/21541248.2014.968004.
53. Feig, L.A. (1999). Tools of the trade: use of dominant-inhibitory mutants of Ras-family GTPases. Nat. Cell Biol. *1*, E25–E27. https://doi.org/10.1038/10018.
54. Gayle, S., Pan, Y., Landrette, S., and Xu, T. (2015). piggyBac insertional mutagenesis screen identifies a role for nuclear RHOA in human ES cell differentiation. Stem Cell Rep. *4*, 926–938. https://doi.org/10.1016/j.stemcr.2015.03.001.
55. Sansom, O.J., Meniel, V.S., Muncan, V., Phesse, T.J., Wilkins, J.A., Reed, K.R., Vass, J.K., Athineos, D., Clevers, H., and Clarke, A.R. (2007). Myc deletion rescues Apc deficiency in the small intestine. Nature *446*, 676–679. https://doi.org/10.1038/nature05674.
56. Sansom, O.J., Reed, K.R., Hayes, A.J., Ireland, H., Brinkmann, H., Newton, I.P., Batlle, E., Simon-Assmann, P., Clevers, H., Nathke, I.S., et al. (2004). Loss of Apc *in vivo* immediately perturbs Wnt signaling, differentiation, and migration. Genes Dev. *18*, 1385–1390. https://doi.org/10.1101/gad.287404.
57. Ordóñez-Morán, P., Larriba, M.J., Pálmer, H.G., Valero, R.A., Barbáchano, A., Duñach, M., de Herreros, A.G., Villalobos, C., Berciano, M.T., Lafarga, M., and Muñoz, A. (2008). RhoA-ROCK and p38MAPK-MSK1 mediate vitamin D effects on gene expression, phenotype, and Wnt pathway in colon cancer cells. J. Cell Biol. *183*, 697–710. https://doi.org/10.1083/jcb.200803020.
58. Leppert, M., Dobbs, M., Scambler, P., O'Connell, P., Nakamura, Y., Stauffer, D., Woodward, S., Burt, R., Hughes, J., and Gardner, E. (1987). The gene for familial polyposis coli maps to the long arm of chromosome 5. Science *238*, 1411–1413. https://doi.org/10.1126/science.3479843.
59. Groden, J., Thliveris, A., Samowitz, W., Carlson, M., Gelbert, L., Albertsen, H., Joslyn, G., Stevens, J., Spirio, L., and Robertson, M. (1991). Identification and characterization of the familial adenomatous polyposis coli gene. Cell *66*, 589–600. https://doi.org/10.1016/0092-8674(81)90021-0.
60. Chawengsaksophak, K., James, R., Hammond, V.E., Köntgen, F., and Beck, F. (1997). Homeosis and intestinal tumours in Cdx2 mutant mice. Nature *386*, 84–87. https://doi.org/10.1038/386084a0.
61. Reitmair, A.H., Redston, M., Cai, J.C., Chuang, T.C., Bjerknes, M., Cheng, H., Hay, K., Gallinger, S., Bapat, B., and Mak, T.W. (1996). Spontaneous intestinal carcinomas and skin neoplasms in Msh2-deficient mice. Cancer Res. *56*, 3842–3849.
62. Edelmann, W., Yang, K., Umar, A., Heyer, J., Lau, K., Fan, K., Liedtke, W., Cohen, P.E., Kane, M.F., Lipford, J.R., et al. (1997). Mutation in the mismatch repair gene Msh6 causes cancer susceptibility. Cell *91*, 467–477. https://doi.org/10.1016/s0092-8674(00)80433-x.
63. Wodarz, A., and Näthke, I. (2007). Cell polarity in development and cancer. Nat. Cell Biol. *9*, 1016–1024. https://doi.org/10.1038/ncb433.
64. Wodarz, A. (2000). Tumor suppressors: linking cell polarity and growth control. Curr. Biol. *10*, R624–R626. https://doi.org/10.1016/s0960-9822(00)00658-8.
65. Partanen, J.I., Nieminen, A.I., and Klefstrom, J. (2009). 3D view to tumor suppression: Lkb1, polarity and the arrest of oncogenic c-Myc. Cell Cycle *8*, 716–724. https://doi.org/10.4161/cc.8.5.7786.
66. Bilder, D., Li, M., and Perrimon, N. (2000). Cooperative regulation of cell polarity and growth by Drosophila tumor suppressors. Science *289*, 113–116. https://doi.org/10.1126/science.289.5476.113.
67. Heng, Y.-W., Lim, H.-H., Mina, T., Utomo, P., Zhong, S., Lim, C.-T., and Koh, C.-G. (2012). TPPP acts downstream of RhoA-ROCK-LIMK2 to regulate astral microtubule organization and spindle orientation. J. Cell Sci. *125*, 1579–1590. https://doi.org/10.1242/jcs.096818.
68. Quyn, A.J., Appleton, P.L., Carey, F.A., Steele, R.J.C., Barker, N., Clevers, H., Ridgway, R.A., Sansom, O.J., and Näthke, I.S. (2010). Spindle orientation bias in gut epithelial stem cell compartments is lost in precancerous tissue. Cell Stem Cell *6*, 175–181. https://doi.org/10.1016/j.stem.2009.12.007.
69. Caldwell, C.M., Green, R.A., and Kaplan, K.B. (2007). APC mutations lead to cytokinetic failures *in vitro* and tetraploid genotypes in Min mice. J. Cell Biol. *178*, 1109–1120. https://doi.org/10.1083/jcb.200703186.
70. Fleming, E.S., Temchin, M., Wu, Q., Maggio-Price, L., and Tirnauer, J.S. (2009). Spindle misorientation in tumors from APC(min/+) mice. Mol. Carcinog. *48*, 592–598. https://doi.org/10.1002/mc.20506.
71. Cartón-García, F., Overeem, A.W., Nieto, R., Bazzocco, S., Dopeso, H., Macaya, I., Bilic, J., Landolfi, S., Hernandez-Losa, J., Schwartz, S., Jr., et al. (2015). Myo5b knockout mice as a model of microvillus inclusion disease. Sci. Rep. *5*, 12312. https://doi.org/10.1038/srep12312.
72. Vanuytsel, T., Vanormelingen, C., Vanheel, H., Masaoka, T., Salim Rasoel, S., Tóth, J., Houben, E., Verbeke, K., De Hertogh, G., Vanden Berghe, P., et al. (2014). From intestinal permeability to dysmotility: the biobreeding rat as a model for functional gastrointestinal disorders. PLoS One *9*, e111132. https://doi.org/10.1371/journal.pone.0111132.

STAR★METHODS

KEY RESOURCES TABLE

REAGENT or RESOURCE	SOURCE	IDENTIFIER
Antibodies		
Mouse monoclonal anti-BrdU	Developmental Studies Hybridoma Bank	Cat#G3G4; RRID: AB_2314035
Rabbit monoclonal anti-Olfm4	Cell Signaling	Cat#D6Y5A; RRID: AB_2650511
Mouse monoclonal anti-β-catenin	BD Biosciences	Cat#610154; RRID: AB_397555
Mouse monoclonal anti-E-cadherin	BD Biosciences	Cat#610181; RRID: AB_397580
Goat polyclonal anti-ezrin	Tebu Bio	Cat#ER-14-0503; RRID: AB_1545407
Mouse monoclonal anti-transferrin receptor (H68.4)	Thermo Fisher Scientific	Cat#13–6800; RRID: AB_2533029
Rabbit polyclonal anti-phospho-ERM (Ezrin, Thr567; Radixin, Thr564; Moesin, Thr558)	Cell Signaling Technology	Cat#3141; RRID: AB_330232
Rabbit polyclonal anti-Cbr3 (Crumbs Cell Polarity Complex Component 3)	Dr. Benjamin L. Margolis Laboratory (University of Michigan Medical School, Ann Arbor, Michigan, USA)	N/A
Rabbit polyclonal anti-lysozyme	Dako	Cat#N1515
Mouse monoclonal anti-RhoA	Cytoskeleton	Cat#ARH03; RRID: AB_10708069
Mouse monoclonal anti-beta tubulin (TUB 2.1)	Sigma-Aldrich	Cat#T4026; RRID: AB_477577
Donkey anti-goat IgG (H + L) Alexa Fluor 594	Thermo Fisher Scientific	Cat#A-11058; RRID: AB_2534105
Goat anti-rabbit IgG (H + L) Alexa Fluor 594	Thermo Fisher Scientific	Cat# A-11012; RRID: AB_2534079
Goat anti-rabbit IgG (H + L) Alexa Fluor 488	Thermo Fisher Scientific	Cat# A-11008; RRID: AB_143165
Goat anti-mouse IgG (H + L) Alexa Fluor 488	Thermo Fisher Scientific	Cat# A-11001; RRID: AB_2534069
Chemicals, peptides, and recombinant proteins		
DAPI (4′, 6-Diamidino-2-phenylindole dihydrochloride)	Biochemica	Cat#A1001
5-Bromo-4-chloro-3-indolyl phosphate p-toluidine	Sigma-Aldrich	Cat#B8503
p-Nitro-Blue tetrazolium chloride	Sigma-Aldrich	Cat#N6876
Levamisole hydrochloride	Santa Cruz Biotechnology	Cat#sc-205730
1-methoxy-5-methylphenazinium methyl sulfate	Sigma-Aldrich	Cat#M8640
Alcian blue 8GX	Sigma-Aldrich	Cat#A5268
p-Nitrophenyl Phosphate Liquid Substrate System	Sigma-Aldrich	Cat#N7653
D-(+)-xylose	Sigma-Aldrich	Cat#X1500
FITC-dextran	Sigma-Aldrich	Cat#FD4
IWR-1-endo	STEMCELL Technologies	Cat#72564
EdU (5-ethynyl-2′-deoxyuridine)	Lumiprobe	Cat#10540
Sulfo-Cy3-Azide	Lumiprobe	Cat#A1330
7-AAD (7-Aminoactinomycin D)	FisherScientific	Cat#10748784
Critical commercial assays		
NovoLink polymer detection system	Leica Biosystems	Cat#RE7280
Dako Fluorescence Mounting Medium	Agilent	Cat#S302380-2
Bouin's solution	Sigma-Aldrich	Cat#HT10132
TRI Reagent	Thermo Fisher Scientific	Cat#AM9738
High Capacity cDNA Reverse Transcription Kit	Applied Biosystems	Cat#4368814
SYBR Select Master Mix	Applied Biosystems	Cat#4472919
TaqMan Universal Master Mix II	Applied Biosystems	Cat#4440047
RhoA Pull-Down Activation Assay Biochem Kit	Cytoskeleton	Cat#BK036

(*Continued on next page*)

Continued

REAGENT or RESOURCE	SOURCE	IDENTIFIER
Experimental models: Cell lines		
Vil-Cre^{+};*RhoA*^{T19N} and *Vil-Cre*$^{-}$;*RhoA*^{T19N} intestinal organoids	This manuscript	N/A
Experimental models: Organisms/strains		
Mouse: *RhoA*^{T19N}: *C57BL/6JJcl-CAT-RhoA-DN/4-18*	RIKEN BioResource Research Center	RRID: IMSR_RBRC01295
Mouse: *Vil-Cre*$^{+}$: *C57BL/6J.SJL-Tg(Vil1-cre)997Gum/J*	The Jackson Laboratory	RRID: IMSR_JAX:018963
Oligonucleotides		
Table S1	This paper	N/A
Software and algorithms		
ImageJ	ImageJ	RRID: SCR_003070
FCS Express 4.0	*De Novo* Software	RRID: SCR_016431
QuPath	QuPath	RRID: SCR_018257

RESOURCE AVAILABILITY

Lead contact

Further information and requests for resources and reagents should be directed to and will be fulfilled by the lead contact Diego Arango (darango@irblleida.cat).

Materials availability

Mouse tissue samples and organoids generated in this study are available from the lead contact upon request, under a Materials Transfer Agreement.

Data and code availability

- Data reported in this paper will be shared by the lead contact upon request.
- This paper does not report original code.
- Any additional information required to reanalyze the data reported in this paper is available from the lead contact upon request.

EXPERIMENTAL MODEL AND STUDY PARTICIPANT DETAILS

Mouse strains and maintenance

All animal experiments were carried out under protocols approved by Vall d'Hebron University Hospital Research Institute Animal Experimentation Ethics Committee. *C57BL/6JJcl-CAT-RhoA-DN/4–18* mice carrying the cytomegalovirus promoter fused to a CAT gene cassette flanked by loxP sites and the dominant negative T19N mutant of *RhoA* were obtained from the RIKEN BioResource Research Center (Starin RBRC01295; hereafter called *RhoA*^{T19N} mice).[28] The *C57BL/6J.SJL-Tg(Vil1-cre)997Gum/J* mice hemizygous for the Villin-Cre transgene expressing *Cre* recombinase under the control of the Villin 1 promoter (hereafter called *Vil-Cre*$^{+}$ mice) were obtained from the Jackson Laboratory (Strain #:004586).[29] Hemizygous *RhoA*^{T19N} mice were crossed with hemizygous *Vil-Cre*$^{+}$ mice, resulting in intestine-specific expression of *RhoAT19N in Vil-Cre*$^{+}$;*RhoA*^{T19N} mice. *Vil-Cre*$^{-}$;*RhoA*^{T19N} mice were used as control in all the experiments. Mouse genotyping was performed with DNA prepared from the mouse ear. Specific PCR primers for RhoA^{T19N} and Vil-Cre were used (Table S1). All experiments included animals from both sexes.

Isolation of mouse intestinal crypts and growth of intestinal organoids

Intestinal crypts were isolated and organoids cultured using IntestiCult Organoid growth medium (STEMCELL Technologies, 06005) following the supplier's instructions. Briefly, 20 cm of the proximal small intestine were dissected, opened longitudinally, cut into 2 mm segments and washed extensively with cold PBS. The intestinal crypts were isolated using 25 mL of Gentle Cell Dissociation Reagent (STEMCELL Technologies, 100–0485) and filtered three times with 100 μm filters. The quality and quantity of the crypt isolation were assessed under the microscope, and 1,500 crypts were resuspended in 300 μL of InstestiCult Organoid growth Medium-Matrigel Basement Membrane Matrix LDEV-free (Corning) solution (1:1). Crypt suspension was plated into low adherence 24-well plates in a drop-wise manner (50 μL/well). The

resulting dome was maintained in InstestiCult Organoid Medium. The medium was replaced 3 times per week and the organoids were routinely passaged every 7–10 days.

METHOD DETAILS

Histology and immunohistochemistry and immunofluorescence

The intestine of 60- and 520-day-old mice was dissected and fixed in 4% formalin. The number and size of macroscopically visible tumors was scored under a dissecting microscope (OLYMPUS SZH stereo-zoom microscope, magnification ×7.5) before paraffin inclusion. For assessment of cell proliferation in tissues, animals were i.p. injected with 100 mg/kg BrdU 2 h before being euthanized, and the number of cells in S-phase was determined by anti-BrdU immunochemical staining (undiluted) following heat induced epitope retrieval (HIER) with 10 mM citrate buffer pH 6.0. For immunohistochemical detection of Olfm4 (1:1000 dilution) and β-catenin (1:500 dilution) HIER was also conducted with citrate buffer, while for lysozyme immunostaining (undiluted) HIER was carried out with 1 mM EDTA at 100°C in for 10 min. All immunohistochemical determinations were conducted with NovoLink polymer detection system. For immunofluorescence antigen retrieval with 10 mM citrate buffer pH 6.0 and the following antibodies were used: E-cadherin (1:100 dilution), ezrin (1:100 dilution), transferrin receptor (1:100 dilution), phospho-ERM T567 (1:100 dilution) and Crb3 (1:100 dilution). Primary antibodies were diluted in blocking solution containing 0.05% Tween 20. Samples were incubated with primary antibodies at 37°C for 2 hours followed by 1 hour incubation with Alexa-Fluor-488-conjugated or Alexa-Fluor-543-conjugated secondary antibodies. Nuclei were counterstained with DAPI and slides mounted with Dako Fluorescent Mounting Medium. Fluorescence microscopy pictures were acquired with a TCS SP8 confocal microscope (Leica DMI 6000).

Histochemical staining

For alkaline phosphatase activity detection, slides were incubated with staining solution for 1 h at 37°C. Then, counterstained with hematoxylin and washed with distilled water before mounting. Staining solution contains 0.4 mg/mL 5-Bromo-4-chloro-3-indolyl phosphate p-toluidine, 0.5 mg/mL p-Nitro-Blue tetrazolium chloride, 100 mM MgCl2, 2 mM Levamisole hydrochloride, 5 mM Sodium azide and 0.15 mM 1-methoxy-5-methylphenazinium methyl sulphate in 100 mM Tris pH 9.5. Enteroendocrine cells were stained using Grimelius silver staining. Briefly, sections were deparaffinized, rehydrated, post-fixed with Bouin's solution for 1 h at 37°C, rinsed once in 70% Ethanol, rinsed twice in distilled water, and immersed in silver solution (0.5% silver nitrate in 0.1 M acetate buffer pH 5.8) for 3–4 h at 60°C. Then, sections were immersed in Bodian solution (5% anhydrous sodium sulfate and 1% hydroquinone in water) for 5 min at 60°C, fixed in 2% sodium thiosulphate, washed in PBS, dehydrated and mounted. Goblet cell staining was performed with 1% Alcian blue in 3% acetic acid for 30 min and counterstained with hematoxylin.

Signal quantification in immunohistochemistry and histochemical stainings

Number of positive cells in the intestinal epithelium of mice was determined by direct count on microscopy images acquired with an AmScope T490B 40X-2000X instrument coupled to a 10MP Digital Camera. For the immunohistochemical analysis of nuclear β-catenin expression, images were obtained with PANNORAMIC 250 Flash III DX digital slide scanner (3D HISTEC), and the intensity nuclear β-catenin staining (3,3′-Diaminobenzidine -DAB) was scored using QuPath software. The staining intensity of all nuclear β-catenin-positive cells of at least 10 intestinal crypts per animal was quantified blinded from sample identity.

Fecal collection from mouse and determination of water content

520-day-old mice were kept individually into empty clean cages for 2 h and fecal pellets collected and weighed. Feces were then dried overnight at 37°C in a dry oven and weighed again to calculate the fecal water content.

Mitotic spindle orientation

The orientation of the mitotic spindle in epithelial cells from the small intestine was determined in hematoxylin and eosin stained sections of *Vil-Cre*$^{+}$;*RhoA*^{T19N} (n = 10 animals; 139 mitosis) and control *Vil-Cre*$^{-}$;*RhoA*^{T19N} mice (n = 8 animals; 155 mitosis) by measuring the angle (alpha) formed by the mitotic spindle during metaphase/anaphase and the epithelial surface using ImageJ software (see Figure 4).

Enzymatic activity assays

Total protein was extracted with mannitol buffer (50 mM D-mannitol, 2 mM Tris and 0.1% Triton X-100). For alkaline phosphatase activity, 50 μg of total protein in 50 μL of mannitol buffer were mixed with 200 μL of p-Nitrophenyl Phosphate Liquid Substrate System, incubated at 37°C for 15 min and the absorbance measured at 405 nm. For the sucrose isomaltase activity assay, 25 μg of total protein in 12.5 μL of mannitol buffer were incubated with 12.5 μL of substrate buffer (0.056 M maltose in mannitol buffer, pH 6.0) at 37°C for 60 min. The reactions were stopped by heating at 100°C for 2 min and the precipitates formed were resuspended in 250 μL of TGO buffer (5 mg horseradish peroxidase, 4 mg glucose oxidase, 10 mg o-dianisidine and 0.2% Triton X-100 in a final volume of 100 mL of Tris 0.5 M, pH 7.0) and the absorbance measured at 450 nm. For the dipeptidylpeptidase IV activity assay, 50 μg of total protein in 90 μL of mannitol buffer were added to 10 μL of 1.4 M glycine-NaOH pH 8.7 and incubated in the presence of 100 μL of substrate buffer (1.5 mM glycyl-L-proline-p-nitroanilide) at 37°C for 30 min. The reactions were stopped with 800 μL of 32% trichloroacetic acid and the samples were centrifuged at 1,700 rpm for 10 min. Then, 50 μL of

supernatants were added to 50 μL of ice-cold 0.2% sodium nitrite and incubated at 4°C for 10 min. Next, 50 μL of 0.5% ammonium sulfamate were added and, after 2 min of incubation, 100 μL of 0.05% n-(1-naphthyl)-ethanediamine were added and incubated at 37°C for 30 min in the dark. The absorbance was measured at 548 nm.

Transmission electron microscopy

Jejunum samples were collected from 90-day-old *Vil-Cre*$^{+}$;*RhoA*^{T19N} (n = 3) and control *Vil-Cre*$^{-}$;*RhoA*^{T19N} mice (n = 3). Samples were fixed with 2.5% glutaraldehyde and 2% paraformaldehyde and processed following standard procedures. Ultra-thin sections were mounted on copper grids, contrasted with uranyle acetate/lead citrate double-staining, and observed in a Jeol JEM-1400 (Jeol LTD) transmission electron microscope equipped with a Gatan Ultrascan ES1000 CCD camera. The brush border architecture was evaluated on at least 12 enterocytes per mouse. Microvillus length and density (microvilli/μm) were measured using ImageJ software as was reported previously.[71]

Determination of D-xylose absorption *in vivo*

To evaluate transcellular transport and epithelial integrity the D-xylose absorption assay was used. Briefly, *Vil-Cre*$^{+}$;*RhoA*^{T19N} (n = 4) and control *Vil-Cre*$^{-}$;*RhoA*^{T19N} mice (n = 4) were fasted for four hours and then, administered 1 mg/g of D-(+)-xylose (100 mg/mL solution) by oral gavage. After 1 hour, peripheral blood samples were collected in BD Microtainer MAP blood collection tubes and D-(+)-xylose levels quantified as previously described.[30] Briefly, 2 mL of phloroglucinol reagent were added to 10 μL plasma and heated for 30 min at 65°C. Samples were allowed to cool to room temperature and the absorbance was measured at 554 nm.

Determination of intestinal permeability *ex vivo*

To evaluate the paracellular permeability and the membrane integrity we used a FITC-dextran of a molecular weight of 4 kDa. Briefly, *Vil-Cre*$^{+}$;*RhoA*^{T19N} (n = 3) and control *Vil-Cre*$^{-}$;*RhoA*^{T19N} mice (n = 3) were fasted for four hours and then, administered 20 mL/kg of FITC-dextran (20 mg/mL solution) by oral gavage. After 3 h, peripheral blood samples were collected in BD Microtainer MAP blood collection tubes and FITC-dextran levels quantified in 200 μL of plasma using a fluorescent plate reader (Appliskan, Thermo Fisher Scientific) set at 485 nm excitation and 535 nm emission.

Determination of intestinal permeability *ex vivo*

Three segments of mid-jejunum and distal colon were mounted in Ussing chambers with an aperture of 0.096 cm^2. The tissue was incubated in 37°C carbogenated Krebs-Ringer bicarbonate buffer and transmucosal potential difference was continuously monitored with Ag/AgCl electrodes. Basal transepithelial electrical resistance (TEER), as a readout of the overall epithelial permeability to ions, was calculated according to Ohm's law from the voltage deflections induced by bipolar constant current pulses of 50μA (every 60s) with duration of 200 ms applied through platinum wires (Mussler Scientific Instruments). A correction for fluid resistance was made. The average TEER was calculated for each animal. FITC-dextran of 4 kDa was added (1 mg/mL) to the apical compartment after an equilibration period to assess the paracelullar permeability. Fluorescence was determined in serial samples collected from the serosal side as previously described.[72] The fluorescence values were converted to ng/ml based on a standard curve. The average cumulative passage of FITC-dextran was calculated for each animal.

Assessment of differentiation in intestinal organoids

Organoid differentiation was assessed by determining the presence of budding crypt-like structures under an inverted phase contrast microscope. When treating organoids with the Wnt inhibitor IWR-1, drug was sustained for 4 consecutive days.

EdU staining of intestinal organoids

Organoids were incubated with 20μM EdU (5-ethynyl-2′-deoxyuridine) for 1 h. Cells were then disaggregated with trypsin, fixed with formalin for 10 min, permeabilized with a solution of 0.1% Triton X-100 in PBS for 10 min, and stained with a solution containing 8μM Sulfo-Cy3-Azide, 2 mM $CuSO_4 \cdot 5H_2O$ and ascorbic acid in PBS. Finally, 7-AAD (7-Aminoactinomycin D) was used as counterstaining. Cells were analyzed with a BD LSRFortessa (BD Biosciences) and FCS Express 4.0 software.

RNA isolation and RT-qPCR

Mice were euthanized and the intestines dissected out, placed on a Whatman filter paper, opened longitudinally and washed with ice-cold PBS. To collect small intestinal epithelial cells, the mucosa was scraped with a cold glass microscope slide and the cells immediately resuspended in 500μL of TRI Reagent. Total RNA was extracted according to the manufacturer's instructions. For RNA extraction of intestinal organoids, cultures were washed with PBS 5 days after seeding and then resuspended in 250 μL of TRI Reagent. Total RNA (500 ng) was

reverse-transcribed using the High-Capacity cDNA Reverse Transcription Kit, and relative expression levels of the following genes were assessed by Real-Time PCR using SYBR Select Master Mix: *RhoA*, CAT Cassette, *c-Myc*, *EphB2*, *Jun* and *Cd44*. Eukaryotic 18S rRNA measured with TaqMan Universal Master Mix II was used for normalization. The sequences of the oligonucleotides used are described in Table S1.

RHOA activity assay

RhoA Pull-Down Activation Assay Biochem Kit (Cytoskeleton) based on GST-tagged Rhotekin-RBD protein was used for determining RHOA activity, according to the manufacturer's instructions.

Western blotting

Total cellular lysates in radioimmunoprecipitation assay (RIPA) buffer were subjected to SDS-PAGE and transferred to PVDF membranes and hybridized using antibodies against human RhoA (1:1,000 dilution) and Tubulin (1:2,500 dilution). Relative RhoA expression was quantified using ImageJ software.

QUANTIFICATION AND STATISTICAL ANALYSIS

Data present means ± SEM, unless otherwise stated. Statistical significance was evaluated using Student's *t* test, Fisher exact test or the Log rank test, and p values were reported as n/s > 0.05, *p < 0.05, **p < 0.01, and ***p < 0.001.